JOURNAL OF AIRCRAFT
Vol. 29, No. 5, Sept.-Oct. 1992

Response of Double-Wall (Sandwich) Circular Plates to Random Excitations—Analytical Approach

Dimitri A. Bofilios*
Integrated Aerospace Sciences Corporation (INASCO), Moschato 18345, Athens, Greece
and
Constantinos S. Lyrintzis†
San Diego State University, San Diego, California 92182

This article presents an analytical approach for the general response of double-wall circular plates subjected to random excitations. The excitations are either uniform random pressures or stationary random point loads. The double-wall construction is separated by a soft linear viscoelastic core. The equations of motion are developed for thin circular plates using Love's theory which has been modified to account for the coupling provided by the viscoelastic core. The analytical solution of forced response is obtained via modal decomposition and a Galerkin-type approach. Numerical results investigate the effect of coupling and structural parameters for response minimization.

Introduction

RECENTLY a variety of circular plates have been extensively used as important structural elements in many transportation structures: aircraft, missiles, launch vehicles, space structures, construction in orbit, and weapons systems. To accommodate many of the requirements, new design concepts are needed. Past studies have demonstrated that sandwich construction might be an effective way of dissipating vibrational energy.[1-5] Therefore, implementation of sandwich construction might prove to be a useful alternative in the design process.

Plate vibration problems have increased in practical importance, and there have been many relevant papers[6,7] and books[8,9] which include complicating factors such as anisotropy, imperfections, elastic foundations, stiffeners, and hygrothermal effects.[10-12] However, most of these studies do not include the sandwich construction of the circular plates.

This paper presents an analytical study and a computational (finite element) verification model for the general response of double-wall circular plates subjected to random excitations. The excitations are either uniform random pressure or a distribution of stationary random point loads that are uncorrelated in space. Both types of loading are characterized by truncated Gaussian white noise spectral densities, i.e., the temporal correlation functions of the excitations are rapidly decaying sinusoidal functions. The double-wall construction is separated by a soft linear viscoelastic core that allows in-phase (flexural) and out-of-phase (dilational) motions of the system.[13-15] The geometric details and location of random point loads are shown in Fig. 1.

The equations of motion, for the analytical approach, are developed for thin circular plates using Love's theory,[16-25] which has been modified to account for the coupling provided by the viscoelastic core.[4,13-15] Since it is assumed that the core is soft, bending and shearing stresses in the core can be neglected, and consequently, its behavior can be described by a uniaxial constitutive law. Furthermore, the inertia effects of the core follow a linearly apportioned mass distribution law. The boundary conditions for the system are taken to be simply supported, which from a physical viewpoint represent either circular knife-edge supports or hinges. Henceforth, the boundary value problem is mathematically defined.

The general solution of forced response is obtained via modal decomposition and a Galerkin-like approach.[4,9,11] Initially, the deflection response is written as a series expansion in terms of time-varying generalized coordinates, and the normal modal eigenfunctions. The modal eigenfunctions are written in terms of Bessel functions, modified Bessel functions, and transcendental functions[26] that are chosen to satisfy the appropriate boundary conditions. The arguments of the Bessel functions constitute solutions to the characteristic frequency equation obtained from the boundary conditions. Using the orthogonality principle of the modal functions, the problem is reduced to a set of coupled differential equations for determining the generalized coordinates. Taking the Fourier transformation of these equations and maximizing the solutions for generalized coordinates, the coupled natural frequencies for the system are obtained. The series solution for the complex response, in the frequency domain, is then given in terms of generalized coordinates and modal eigenfunctions. The spectral density of the response can be estimated by taking the mathematical expectation of the solution series.[27]

The finite element model employs the NASTRAN finite element code.[28] It consists of 1026 nodes (6156 dof) and 1529

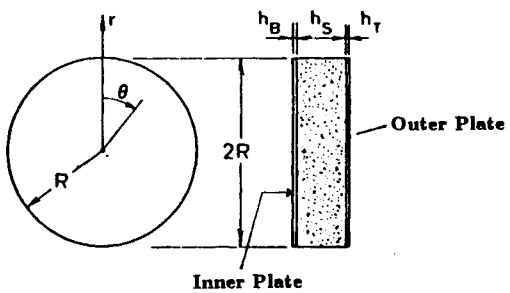

Fig. 1 Double-wall circular plate.

Received Jan. 14, 1991; revision received June 5, 1991; accepted for publication Sept. 9, 1991.

*Technical Director, Department of Research and Development, 22 Miaouli Street.
†Associate Professor, Department of Aerospace Engineering and Engineering Mechanics. Member AIAA.

two-dimensional elements. The viscoelastic core is modeled using spring stiffness elements. An eigenvalue modal analysis (SOL 3) is performed where the natural frequencies and modal shapes are determined and compared to the closed formed solutions.

This paper contains deflection response spectral densities for uniform random pressure exitation and random point loads, as well as mode shapes and frequencies, and comparisons between the analytical and the computational (finite element) approaches. The results show very good agreement. It is also shown that with proper selection of the dynamic characteristics the response levels can be reduced.

Analytical Model

Consider the two circular plates shown in Fig. 1 that are simply supported around the edges. The boundary conditions for deflection and radial bending moment at the edges are

$$w_{T,B}(r, \theta) = 0 \quad \text{at} \quad r = R \tag{1}$$

$$M_r(r, \theta) = -D_{T,B}\left\{\frac{\partial^2 w_{T,B}}{\partial r^2} + \nu_{T,B} \cdot \left(\frac{1}{r}\frac{\partial w_{T,B}}{\partial r} + \frac{1}{r^2}\frac{\partial^2 w_{T,B}}{\partial \theta^2}\right)\right\} = 0 \quad \text{at} \quad r = R \tag{2}$$

where $w_{T,B}$ are the normal displacements of the midsurfaces of the top (exterior) and bottom (interior) circular plates respectively. R is the plate radius, $\nu_{T,B}$ is the Poisson's ratio for the top and bottom plate. $D_{T,B}$ are the top and bottom plate rigidities which are given as

$$D_{T,B} = \frac{E_{T,B}h_{T,B}^3}{12(1 - \nu_{T,B}^2)} \tag{3}$$

in which $E_{T,B}$ are the elastic modulii, and $h_{T,B}$ are the thicknesses of outer and inner circular plates. The governing equations of motion of the two plates, coupled through a linear soft core, can be written as[4,13,16,17]

$$D_T\nabla^4 w_T + c_T\dot{w}_T + m_T\ddot{w}_T + k_s(w_T - w_B) + \tfrac{1}{3}m_s\ddot{w}_T + \tfrac{1}{6}m_s\ddot{w}_B = -p_T(r, \theta, t) \tag{4}$$

$$D_B\nabla^4 w_B + c_B\dot{w}_B + m_B\ddot{w}_B + k_s(w_B - w_T) + \tfrac{1}{3}m_s\ddot{w}_B + \tfrac{1}{6}m_s\ddot{w}_T = p_B(r, \theta, t) \tag{5}$$

where

$$m_{T,B} = \rho_{T,B}h_{T,B} \tag{6}$$

$$m_s = \rho_s h_s \tag{7}$$

$$\nabla^4 = \left(\frac{\partial^2}{\partial r^2} + \frac{1}{r}\frac{\partial}{\partial r} + \frac{1}{r^2}\frac{\partial^2}{\partial^2\theta}\right)\left(\frac{\partial^2}{\partial r^2} + \frac{1}{r}\frac{\partial}{\partial r} + \frac{1}{r^2}\frac{\partial^2}{\partial^2\theta}\right) \tag{8}$$

The subscripts $_{T,B}$ denote the top and bottom plates and s denotes the core. The pressures $p_T(r, \theta, t)$ and $p_B(r, \theta, t)$ are the random excitations applied to the top and bottom plates. $c_{T,B}$, $m_{T,B}$ and $\rho_{T,B}$ are the damping coefficients, surface densities, and mass densities of the circular plates, respectively. m_s, and ρ_s are the surface density and mass density of the soft core. The stiffness of the core is represented by a linear viscoelastic spring, $k_s = k_0(1 + ig_s)$, where k_0 is the spring constant, g_s is the loss factor, and $i = \sqrt{-1}$. In obtaining Eqs. (4) and (5) it was assumed that the mass of the core follows an apportioned linear distribution.

The solution to Eqs. (4) and (5) can be expressed in terms of normal modes

$$w_T(r, \theta, t) = \sum_{s=0}^{\infty}\sum_{q=1}^{\infty} {}_TA_{sq}(t)\, X_{sq}(r, \theta) \tag{9}$$

$$w_B(r, \theta, t) = \sum_{s=0}^{\infty}\sum_{q=1}^{\infty} {}_BA_{sq}(t)\, X_{sq}(r, \theta) \tag{10}$$

where ${}_TA_{sq}$ and ${}_BA_{sq}$ are the generalized coordinates of top (exterior) and bottom (interior) circular plates, and $X_{sq}(r, \theta)$ are the circular plate modes. These modes have to satisfy the boundary conditions. Thus, we may choose a combination of Bessel and modified Bessel functions in the radial direction, and a cosine function in the tangential direction. The function in the radial direction has to satisfy Eq. (1), which leads to circular plate modes given by

$$X_{sq} = R_{sq}(r)\cos(s\theta) \tag{11}$$

where

$$R_{sq}(r) = J_s(k_{sq}r) - \frac{J_s(\lambda_{sq})}{I_s(\lambda_{sq})}I_s(k_{sq}r) \tag{12}$$

in which J_s and I_s, are Bessel functions and modified Bessel functions of the first kind respectively, and λ_{sq} is the qth root of the frequency equation

$$\frac{J_{s+1}(\lambda)}{J_s(\lambda)} + \frac{I_{s+1}(\lambda)}{I_s(\lambda)} = \frac{2\lambda}{1 - \nu} \tag{13}$$

Equation (13) is obtained by substituting Eqs. (11) and (12) into Eqs. (1) and (2) and using relationships which relate the derivatives of Bessel functions to high order functions, along with Bessel recurrence formulas.[18,23,26] Some details of the derivation are given in Appendix A. In equation (13) $\lambda = kR$, $k^4 = \omega^2 m/D$ and consequently

$$\lambda_{sq} = k_{sq}R \tag{14}$$

$$k_{sq}^4 = {}_{T,B}\omega_{sq}^2 m_{T,B}/D_{T,B} \tag{15}$$

Substituting Eqs. (9) and (10) into Eqs. (4) and (5) and using the orthogonality principle (see also Appendix B), gives a set of coupled differential equations in ${}_TA_{sq}$ and ${}_BA_{sq}$. Taking the Fourier transform of these equations it can be shown that

$${}_T\bar{A}_{sq}(\omega) = \frac{{}_TH_{sq}(\omega)}{m_T}\cdot\left\{{}_B\bar{A}_{sq}(\omega)\left(k_s + \frac{1}{6}m_s\omega^2\right) + \frac{{}_T\bar{P}_{sq}(\omega)}{\bar{Q}_{sq}}\right\} \tag{16}$$

$${}_B\bar{A}_{sq}(\omega) = \frac{{}_BH_{sq}(\omega)}{m_B}\cdot\left\{{}_T\bar{A}_{sq}(\omega)\left(k_s + \frac{1}{6}m_s\omega^2\right) + \frac{{}_B\bar{P}_{sq}(\omega)}{\bar{Q}_{sq}}\right\} \tag{17}$$

where

$${}_{T,B}H_{sq}(\omega) = \frac{1}{{}_{T,B}\omega_{sq}^2 - \omega^2\dfrac{\gamma_{T,B}}{m_{T,B}} + i\omega\dfrac{c_{T,B}}{m_{T,B}} + \dfrac{k_s}{m_{T,B}}} \tag{18}$$

$$\gamma_{T,B} = m_{T,B} + \tfrac{1}{3}m_s \tag{19}$$

$${}_{T,B}\bar{P}_{sq}(\omega) = \mp\int_0^R\int_0^{2\pi} p_{T,B}(r, \theta, \omega)\, X_{sq}(r, \theta)\, r\, dr\, d\theta \tag{20}$$

$$\bar{Q}_{sq} = \int_0^R \int_0^{2\pi} [X_{sq}(r, \theta)]^2 \, r \, dr \, d\theta = \begin{cases} \pi Q_{sq} & \text{if } s \neq 0 \\ 2\pi Q_{sq} & \text{if } s = 0 \end{cases} \tag{21}$$

and

$$Q_{sq} = \frac{R^2}{2}\left\{J_s'^2(\lambda_{sq}) + \left(1 - \frac{s^2}{\lambda_{sq}^2}\right) J_s^2(\lambda_{sq})\right\} - \frac{R^2}{\lambda_{sq}} \frac{J_s(\lambda_{sq})}{I_s(\lambda_{sq})}\left\{I_s'(\lambda_{sq}) J_s(\lambda_{sq}) - J_s'(\lambda_{sq}) I_s(\lambda_{sq})\right\} + \frac{R^2}{2} \frac{J_s^2(\lambda_{sq})}{I_s^2(\lambda_{sq})}\left\{\left(1 + \frac{s^2}{\lambda_{sq}^2}\right) I_s^2(\lambda_{sq}) - I_s'^2(\lambda_{sq})\right\} \tag{22}$$

$$_{T,B}\omega_{sq}^2 = k_{sq}^4 D_{T,B}/m_{T,B} \tag{23}$$

Furthermore, a ( )′ indicates differentiation with respect to the spatial variable r, and a bar indicates transformed quantity. Equations (21) and (22) represent the orthogonality condition, which involves integrations of combinations of Bessel and Modified Bessel functions. Details of the orthogonality condition are offered in Appendix B.

The coupled natural frequencies ω_{sq}^c are the points at which the relative maxima of Eq. (18) occur. This in turn suggests that the relative maxima of the coupled Eqs. (16) and (17) should be determined. Thus, the procedure to obtain the frequencies starts by setting $c_T = c_B = g_s = 0$ in Eq. (18) and substitute (18) into (16) and (17). Then, eliminating $_B\bar{A}_{sq}(\omega)$ from Eq. (16) results in a fourth-order equation for the coupled frequencies ω_{sq}^c, whose solution is

$$\omega_{sq}^c = \left\{\frac{1}{2a}\left[-b_{sq} \pm (b_{sq}^2 - 4a \, d_{sq})^{1/2}\right]\right\}^{1/2} \tag{24}$$

where

$$a = \gamma_T \gamma_B - (\tfrac{1}{6} m_s)^2 \tag{25}$$

$$b_{sq} = (_T\omega_{sq}^2 \rho_T + k_s)\gamma_B + (_B\omega_{sq}^2 \rho_B + k_s)\gamma_T + k_s m_s/3 \tag{26}$$

$$d_{sq} = (_T\omega_{sq}^2 \rho_T + k_s)(_B\omega_{sq}^2 \rho_B + k_s) - k_s^2 \tag{27}$$

Equation (24) gives two characteristic values for each set of modal indices (s, q). These roots are associated with in-phase flexural and out-of-phase dilatational vibration frequencies of the sandwich construction.

The excitations applied to the top and/or bottom circular plates are assumed to be uniform random pressure or random point loads as shown in Fig. 2 for which the spectral densities are specified. In the case of uniform pressure input the generalized random forces reduced to

$$_{T,B}\bar{P}_{sq}(\omega) = \begin{cases} 2\pi\mu_{0q}\bar{p}_{T,B}(\omega) & \text{if } s = 0 \\ 0 & \text{if } s \neq 0 \end{cases} \tag{28}$$

where

$$\mu_{0q} = \frac{R}{k_{0q}}\left\{J_1(\lambda_{0q}) - \frac{J_0(\lambda_{0q})}{I_0(\lambda_{0q})} I_1(\lambda_{0q})\right\} \tag{29}$$

and $\bar{p}_{T,B}(r, \theta, \omega)$ is the Fourier transform for spatially uniform pressure input $p_{T,B}(r, \theta, t)$.

The random loads acting on the top and bottom plates are expressed in terms of two point loads $F_1^{T,B}$ and $F_2^{T,B}$ as

$$p_T(r, \theta, t) = \frac{1}{A_1^T A_2^T}\{F_1^T(t)\,\delta(\theta - \theta_1^T)\,\delta(r - r_1^T) + F_2^T(t)\,\delta(\theta - \theta_2^T)\,\delta(r - r_2^T)\} \tag{30}$$

$$p_B(r, \theta, t) = \frac{1}{A_1^B A_2^B}\{F_1^B(t)\,\delta(\theta - \theta_1^B)\,\delta(r - r_1^B) + F_2^B(t)\,\delta(\theta - \theta_2^B)\,\delta(r - r_2^B)\} \tag{31}$$

where $_{T,B}$ denote the external and internal loads, δ is the Dirac delta function and for a circular plate[29] $A_1^{B,T} = 1$, $A_2^{B,T} = r$. Also, $r_1^{T,B}$, $\theta_1^{T,B}$ and $r_2^{T,B}$, $\theta_2^{T,B}$ correspond to the position of load $F_1^{T,B}$ and $F_2^{T,B}$ respectively. The generalized random forces corresponding to point loads given in Eqs. (30) and (31) are

$$_T\bar{P}_{sq}(\omega) = \{\bar{F}_1^T(\omega)\, X_{sq}(r_1^T, \theta_1^T) + \bar{F}_2^T(\omega)\, X_{sq}(r_2^T, \theta_2^T)\} \tag{32}$$

$$_B\bar{P}_{sq}(\omega) = \{\bar{F}_1^B(\omega)\, X_{sq}(r_1^B, \theta_1^B) + \bar{F}_2^B(\omega)\, X_{sq}(r_2^T, \theta_2^B)\} \tag{33}$$

Following the procedures of Ref. 27 and assuming the point loads are stationary and independent, the spectral densities of normal plate deflections w_T, w_B can be determined from

$$_{T,B}S_w(r, \theta, \omega) = \sum_{s=0}^{\infty}\sum_{q=1}^{\infty}\sum_{j=0}^{\infty}\sum_{k=1}^{\infty}\{_{T,B}\Theta_{sq}\,(_{T,B}\Theta_{jk}^*)\,_{T,B}S_{sqjk}(\omega) + \Lambda_{sq}\,(\Lambda_{jk}^*)\,_{B,T}S_{sqjk}\}\frac{X_{sq}X_{jk}}{\bar{Q}_{sq}\bar{Q}_{jk}} \tag{34}$$

where

$$_{T,B}\Theta_{sq}(\omega) = \frac{_{T,B}H_{sq}(\omega)}{m_{T,B}\Phi_{sq}} \tag{35}$$

$$\Lambda_{sq}(\omega) = {}_T\Theta_{sq}(\omega)\left(\frac{_BH_{sq}(\omega)}{m_B}\right)\left(k_s + \frac{1}{6} m_s\omega^2\right) \tag{36}$$

$$\Phi_{sq}(\omega) = 1 - \frac{_TH_{sq}(\omega)\,_BH_{sq}(\omega)\,(k_s + \frac{1}{6}m_s\omega^2)^2}{m_T m_B} \tag{37}$$

The asterisks in Eq. (34) denote complex conjugates, and $_{B,T}S_{sqjk}$ are the cross-spectral densities of the generalized random forces.

For two stationary independent point loads acting on the external plate, using Eqs. (32) and (33) it may be shown[4] that the cross-spectral density of the generalized forces $_TS_{sqjk}(\omega)$ may be determined from

$$_TS_{sqjk}(\omega) = \{S_{F_1}^T(\omega)\, X_{sq}(r_1^T, \theta_1^T)\, X_{jk}(r_1^T, \theta_1^T) + S_{F_2}^T(\omega)\, X_{sq}(r_2^T, \theta_2^T)\, X_{jk}(r_2^T, \theta_2^T)\} \tag{38}$$

where $S_{F_1}^T$ and $S_{F_2}^T$ are the spectral densities of the point loads F_1^T and F_2^T. Similar expressions can be developed for point loads acting on the interior plate.

Numerical Results

Numerical results presented herein are for a double-wall circular plate as the one shown in Figs. 1 and 2.

The dimensions of the double-wall circular plates are taken to the radius $R = 58$ in., core thickness $h_s = 2$ in. The

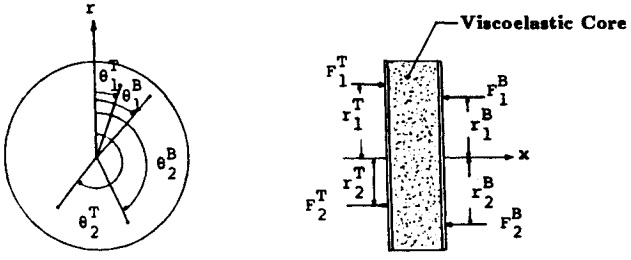

Fig. 2 Location of random point loads.

thicknesses of the inner and outer plates are $h_T = h_B = 0.25$ in. The stiffness and material density of the core are, $k_s = 4.17\ lb_f/\text{in.}^3$ and $\rho_s = 3.4 \times 10^6\ lb_f - s^2/\text{in.}^4$. Both end plate systems are composed of aluminum, with elastic moduli $E_T = E_B = 10.5 \times 10^6$ psi, Poisson's ratios $\nu_T = \nu_B = 0.3$ and material densities $\rho_T = \rho_B = 0.000259\ lb_f - s^2/\text{in.}^4$. The viscous damping coefficients c_T and c_B are expressed in terms of modal damping ratios ζ_{sq}^T and ζ_{sq}^B corresponding to the outer (top) and inner (bottom) plates, respectively. The loss factor accounting for damping in the soft core of the double-wall plate system is taken to be $g_s = 0.02$.

The input random pressures p_T, p_B, and the point loads F_j^T, F_j^B $(j = 1, 2)$ are assumed to be characterized by truncated Gaussian white noise spectral densities.

$$S_{p_T,p_B} = \begin{cases} 8.41 \times 10^{-7}\ (\text{psi})^2/\text{Hz} & 0 < f < 1000\ \text{Hz} \\ 0 & \text{otherwise} \end{cases} \tag{39}$$

$$S_{F_1,F_2}^{T,B} = \begin{cases} 0.84\ lb_f^2/\text{Hz} & 0 < f < 1000\ \text{Hz} \\ 0 & \text{otherwise} \end{cases} \tag{40}$$

The spectral densities given in Eq. (39) correspond to a 100 dB sound level. The magnitudes of input point loads characterized by spectral densities given in Eqs. (39) and (40) were selected in such a way that the resulting maximum circular plate response is linear and equal to about one-half the value of the outer plate thickness.

The core separating the double-wall end plate construction is taken to be relatively soft in order to allow for dilational modes to be present. The coupled modal frequencies of the double wall aluminum caps for $s = 0, 1, 2, 3$ (number of nodal diameters) and $q = 1, 2, \ldots 10$ (number of nodal circles) are given in Table 1 where F, D represent the in phase (flexural) and out of phase (dilatational) motions of the double-wall circular plates, respectively. The natural frequencies are not in increasing order. The first mode corresponds to $s = 0$ (no nodal diameters) and $q = 1$ (one nodal circle); the second mode to $s = 1$, $q = 1$; the third mode to $s = 2$, $q = 1$, etc. The frequency of the first dilatational mode comes after seven flexural modes have occurred. The first three structural modes for zero number of diametrical nodes are shown in Fig. 3.

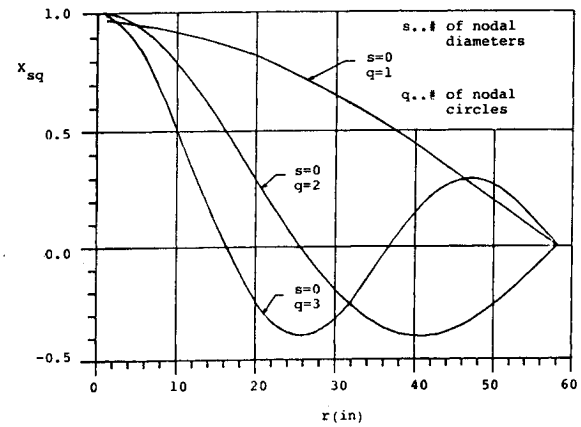

Fig. 3 First structural mode of the double-wall circular plate (finite element solution).

Table 1 Coupled modal frequencies

s	q	D, Hz	F, Hz	s	q	D, Hz	F, Hz
0	1	57.4517	3.5678	2	1	60.2477	18.4883
0	2	61.2197	21.4450	2	2	76.4402	50.5483
0	3	78.4144	53.4869	2	3	112.5142	96.8064
0	4	115.1318	99.8367	2	4	167.5470	157.4294
0	5	169.9609	159.9963	2	5	238.6752	231.6849
0	6	241.6965	234.7966	2	6	325.9345	320.8490
0	7	328.6345	323.5924	2	7	427.6605	423.8004
0	8	430.4361	426.6012	2	8	544.0834	541.0486
0	9	547.2275	544.2151	2	9	675.0477	672.6002
0	10	678.5546	576.1352	2	10	820.9465	818.9479
1	1	58.2062	9.9993	3	1	64.1809	28.8309
1	2	67.1581	34.9606	3	2	89.0700	68.1579
1	3	93.6944	74.0991	3	3	134.2777	121.4190
1	4	139.7819	127.4795	3	4	197.6342	189.1329
1	5	203.0434	194.7783	3	5	276.9535	270.9519
1	6	282.4519	276.5709	3	6	371.2432	366.7382
1	7	377.0500	372.6645	3	7	480.5413	477.1080
1	8	486.0809	482.6870	3	8	604.2222	601.4952
1	9	610.0399	607.3391	3	9	742.9498	740.7407
1	10	748.0262	745.8323	3	10	895.3002	893.4334

s = number of nodal diameters; q = number of nodal circles; F = flexural frequencies (Hz); D = dilatational frequencies (Hz).

A finite element was obtained to verify the theoretical results. The NASTRAN finite element code was used. The model consists of 1026 nodes (6156 degrees of freedom) and 1529 two-dimensional elements. The viscoelastic core of the sandwich construction is modeled using spring stiffness elements. The fundamental frequency obtained by the finite element model is 3.60 Hz, and the corresponding modal shape is depicted in Fig. 4. It corresponds to an in-plane overall bending mode with zero nodal diameters and one modal circle (boundary). The corresponding theoretical value ($s = 0$, q

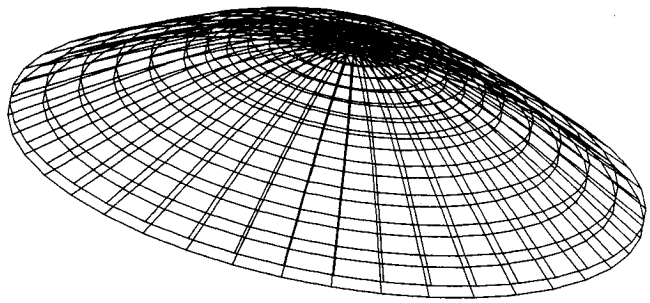

Fig. 4 Second structural mode of the double-wall circular plate (finite element solution).

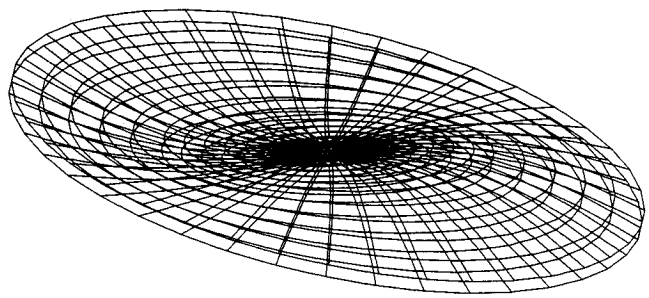

Fig. 5 Structural modes of circular plates.

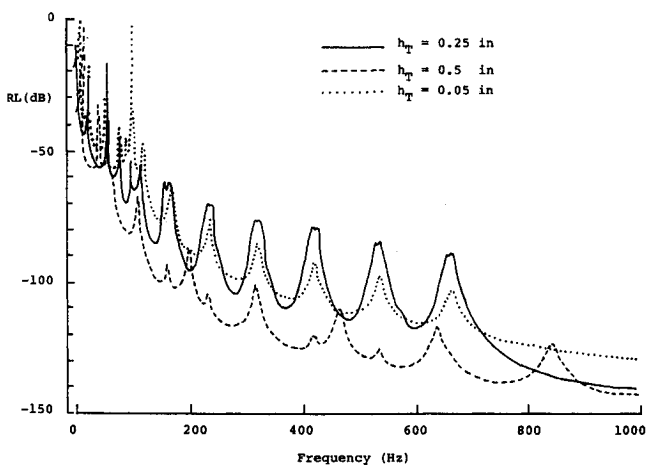

Fig. 6 Deflection of inner plate for different thicknesses of the outer plate.

= 1 in Table 1) is 3.57 Hz. The second mode is at 10.1 Hz (closed form solution is 9.99 Hz) and shown in Fig. 5. The second mode corresponds to one nodal diameter and one nodal circle. Very good agreement was found for all the next 10 modes. The values for the frequency from the finite element model and the theoretical one are almost identical to the first decimal point. From these results it is evident that there is excellent agreement between the closed form and the finite element predictions (at least at the lower frequency range).

The response level (RL), in units of decibels (dB), for the top (exterior) or bottom (interior) plate of the sandwich construction can be evaluated using

$$\mathrm{RL}^{T,B}(r, \theta, \omega) = 10 \log \left\{ \frac{{}_{T,B}S_w(r, \theta, \omega)\, \Delta\omega}{w_{\mathrm{rel}}^2} \right\} \quad (41)$$

where the reference deflection w_{rel} is taken to be $w_{\mathrm{rel}} = 0.032$ in.

The response levels, as given by Eq. (41), of the inner plate of the double-wall end cap construction are illustrated in Fig. 6 for various thicknesses of the outer plate. These results are for a uniform random pressure input, as given by Eq. (39), acting on the other plate. The modal damping ratios are assumed to be constant, $\zeta_{sq}^T = \zeta_{sq}^B = \zeta_0 = 0.06$, and the loss factor in the core $g_s = 0.02$. The thickness of the inner plate was taken to be $h_B = 0.25$ in. For a uniform random pressure excitation, only the modes with $s = 0$ (i.e., no nodal diameters) are excited. As can be seen from Fig. 6, the response levels of the inner plate are significantly higher at most values of the lower frequency range when the thickness of the outer plate is $h_T = 0.05$ in. However, the trend is reversed when the thickness of the outer plate increases to $h_T = 0.25$ in. and $h_T = 0.5$ in. It should be noted that for $h_T = 0.05$ in., the response level of the inner plates almost reaches the nonlinear range, and, therefore, assumptions made in the formulation of the theory may be violated. At higher frequency values and $h_T = 0.5$ in., significantly lower response levels for the inner plate are observed.

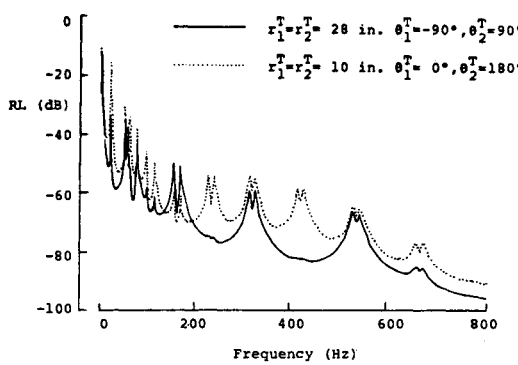

Fig. 7 Response levels of outer plate for different location of point loads (exterior).

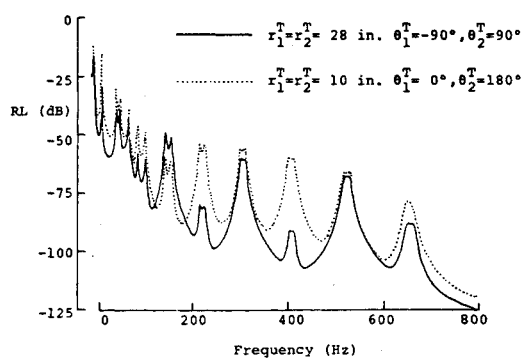

Fig. 8 Response levels of inner plate for different location of point loads (exterior).

The effect on structural response due to changes in location of point loads is presented in Figs. 7 and 8. In this case, the thicknesses of the plates are taken to be $h_T = h_B = 0.25$ in. The two point loads are acting on the outer plate and characterized by the spectral densities given in Eq. (40). The response levels for both the inner and outer plates are calculated at $r = 0$ in. (i.e., at the center of the plate) and $\theta = 45$ deg. In Fig. 7 results are presented for the outer plate response due to two point loads acting on $r_1^T = r_2^T = 28$ in. $\theta_1^T = -90$ deg, $\theta_2^T = 90$ deg, and $r_1^T = r_2^T = 10$ in. $\theta_1^T = 0$ deg, $\theta_2^T = 180$ deg. As can be seen from these results, response levels are significantly higher at most modal frequencies when the point loads are located at $r_1^T = r_2^T = 10$ in. and $\theta_1^T = 0$ deg, $\theta_2^T = 180$ deg. Furthermore, the number of participating modes in the response calculation is increased. However, the response level at the fundamental modal frequency (3.73 Hz) is approximately the same for both of these cases. In Fig. 8, results are presented for the vibration response of the inner plate. From the results shown in Figs. 7 and 8 it can be said that at the first two modal frequencies the response levels for both the inner and outer plates are about the same and not strongly dependent on the location of point load application.

Conclusions

An analytical model has been developed to predict the forced response of double-wall circular plate constructions to random loading. Results indicate that response levels are sensitive to the nature of loading (i.e., uniform or point loads) and the properties of the viscoelastic core. Coupling of the plates, due to structural parameter fluctuations, can also be used to tailor the response of the sandwich construction. Different material characteristics or different geometry may be used to relocate some of the response peaks and reduce their amplitude. However, only specific frequency ranges will be affected. For example, thinner plates tend to amplify the response at low frequencies while having an opposite effect at higher frequencies. Finally, the response levels do not seem to be strongly dependent on the location of point load application, as expected.

Appendix A: Frequency Equation

The displacement solution in terms of normal modes is given in Eqs. (9) and (10) as

$$w_{T,B}(r, \theta, t) = \sum_{s=0}^{\infty} \sum_{q=1}^{\infty} {}_{T,B}A_{sq}(t)\, X_{sq}(r, \theta) \quad (A1)$$

where

$$X_{sq}(r, \theta) = \left\{ J_s(k_{sq}r) - \frac{J_s(\lambda_{sq})}{I_s(\lambda_{sq})} I_s(k_{sq}r) \right\} \cos(s\theta) \quad (A2)$$

The frequency equation can be determined by substituting Eq. (A1) into the boundary condition [same as Eq. (2)]

$$M_r(r, \theta) = -D_{T,B} \cdot \left\{ \frac{\partial^2 w_{T,B}}{\partial r^2} + \nu_{T,B} \left(\frac{1}{r} \frac{\partial w_{T,B}}{\partial r} + \frac{1}{r^2} \frac{\partial^2 w_{T,B}}{\partial \theta^2} \right) \right\} = 0 \quad \text{at} \quad r = R \quad (A3)$$

The substitution will involve first and second derivatives of the Bessel and modified Bessel functions. Recurrence formulas for Bessel functions and Lommel's polynomial can be used to simplify the expression. The following expressions can be proved using basic recurrene formulas:

$$J_{s+2}(z) = \frac{2(s+1)}{z} J_{s+1}(z) - J_s(z) \quad (A4)$$

$$J_{s-2}(z) = \frac{2(s-1)}{z} J_{s-1}(z) - J_s(z) \quad \text{(A5)}$$

$$I_{s+2}(z) = I_s(z) - \frac{2(s+1)}{z} I_{s+1}(z) \quad \text{(A6)}$$

$$I_{s-2}(z) = I_s(z) + \frac{2(s-1)}{z} I_{s-1}(z) \quad \text{(A7)}$$

$$J'_s(z) = \frac{a}{z} J_s(z) - J_{s+1}(z) \quad \text{(A8)}$$

$$I'_s(z) = \frac{a}{z} I_s(z) + I_{s+1}(z) \quad \text{(A9)}$$

$$J''_s(z) = \frac{1}{z} J_{s+1}(z) + J_s(z) \left[\frac{s(s-1)}{z^2} - 1 \right] \quad \text{(A10)}$$

$$I''_s(z) = \frac{1}{z} J_{s+1}(z) + J_s(z) \left[\frac{s(s-1)}{z^2} + 1 \right] \quad \text{(A11)}$$

Using Eqs. (A4)–(A11), the frequency equation can be written as

$$\frac{J_{s+1}(\lambda_{sq})}{J_s(\lambda_{sq})} + \frac{I_{s+1}(\lambda_{sq})}{I_s(\lambda_{sq})} = \frac{2\lambda_{sq}}{1-\nu} \quad \text{(A12)}$$

where $\lambda_{sq} = k_{sq}R$.

Appendix B: Orthogonality Condition

Substituting the displacements in terms of normal modes [i.e., Eqs. (9) and (10)] into the governing Eqs. (4) and (5), the orthogonality principle has to be used to eliminate the summations. This means that all terms of the resulting equations are multipled by $rR_{mn}(r)\cos m\theta$, and integrated from 0 to 2π (tangential direction) and from 0 to R (radial direction). Thus the orthogonality condition has the following form

$$\int_0^R \int_0^{2\pi} X_{sq}(r,\theta)\, X_{mn}(r,\theta)\, r\, dr\, d\theta \quad \text{(B1)}$$

where

$$X_{sq} = R_{sq}(r)\cos(s\theta) \quad \text{(B2)}$$

$$R_{sq}(r) = J_s(k_{sq}r) - \frac{J_s(\lambda_{sq})}{I_s(\lambda_{sq})} I_s(k_{sq}r); \quad \lambda_{sq} = k_{sq}R \quad \text{(B3)}$$

However, since

$$\int_0^{2\pi} \cos(s\theta)\cos(m\theta)\, d\theta = \begin{cases} \pi & \text{if } s = m \neq 0 \\ 2\pi & \text{if } s = m = 0 \\ 0 & \text{if } s \neq m \end{cases} \quad \text{(B4)}$$

the following integral has to be determined

$$\int_0^R R_{sq}(r) R_{sn}(r) r\, dr \quad \text{(B5)}$$

Substituting Eq. (B3) into (B5), the use of Eq. (B6) is needed.

$$\int_0^R r\mathcal{L}_\alpha(\beta r)\, \mathcal{D}_\alpha(\gamma r)\, dr = \frac{R}{\beta^2 - \gamma^2} \cdot \left[\beta\mathcal{L}_{\alpha+1}(\beta R)\, \mathcal{D}_\alpha(\gamma R) - \gamma\mathcal{L}_\alpha(\beta R)\, \mathcal{D}_{\alpha+1}(\gamma R) \right] \quad \text{(B6)}$$

where $\mathcal{L}$ and $\mathcal{D}$ are any cylindrical functions. Using Eq. (B6), it can be found that the integral in Eq. (B5) is equal to zero if $q \neq n$. Thus, again using Eq. (B6) along with L' Hospital's rule (because $q = n$), and the recurrence relations presented in Appendix A, and a back substitution into the Bessel equation, the following results can be obtained.

$$\int_0^R r J_s^2(k_{sq}r)\, dr = \frac{R^2}{2} \left\{ J_s'^2(\lambda_{sq}) + \left(1 - \frac{s^2}{\lambda_{sq}^2}\right) J_s^2(\lambda_{sq}) \right\} \quad \text{(B7)}$$

$$\int_0^R r I_s^2(k_{sq}r)\, dr = \frac{R^2}{2} \left\{ \left(1 + \frac{s^2}{\lambda_{sq}^2}\right) I_s^2(\lambda_{sq}) - I_s'^2(\lambda_{sq}) \right\} \quad \text{(B8)}$$

$$\int_0^R r J_s(k_{sq}r)\, I_s(k_{sq}r)\, dr = \frac{R^2}{2\lambda_{sq}} \left\{ I'_s(\lambda_{sq})\, J_s(\lambda_{sq}) - J'_s(\lambda_{sq})\, I_s(\lambda_{sq}) \right\} \quad \text{(B9)}$$

Thus, using all the obtained results, the orthogonality condition reads

$$\int_0^R \int_0^{2\pi} X_{sq}(r,\theta)\, X_{mn}(r,\theta)\, r\, dr\, d\theta = \begin{cases} \pi Q_{sq} & \text{if } q = n,\ s = m \neq 0 \\ 2\pi Q_{sq} & \text{if } q = n,\ s = m = 0 \\ 0 & \text{if } q \neq n \text{ or } s \neq m \end{cases} \quad \text{(B10)}$$

where

$$Q_{sq} = \int_0^R R_{sq}^2(r)\, r\, dr = \frac{R^2}{2} \left\{ J_s'^2(\lambda_{sq}) + \left(1 - \frac{s^2}{\lambda_{sq}^2}\right) J_s^2(\lambda_{sq}) \right\} - \frac{R^2}{\lambda_{sq}} \frac{J_s(\lambda_{sq})}{I_s(\lambda_{sq})} \cdot \left\{ I'_s(\lambda_{sq})\, J_s(\lambda_{sq}) - J'_s(\lambda_{sq})\, I_s(\lambda_{sq}) \right\} + \frac{R^2}{2} \frac{J_s^2(\lambda_{sq})}{I_s^2(\lambda_{sq})} \cdot \left\{ \left(1 + \frac{s^2}{\lambda_{sq}^2}\right) I_s^2(\lambda_{sq}) - I_s'^2(\lambda_{sq}) \right\} \quad \text{(B11)}$$

Acknowledgment

C. Lyrintzis was supported in part by a grant from the San Diego State University Foundation.

References

[1]Bieniek, M. P., and Freudenthal, M. A., "Frequency Response Functions of Orthotropic Sandwich Plates," *Journal of Aerospace Sciences,* Vol. 28, No. 9, 1961, pp. 732–735, 752.

[2]Freudenthal, M. A., and Bieniek, M. P., "Forced Vibrations of Sandwich Structures," WADD Technical Rept. 60-307, U.S. Air Force, Jan. 1961.

[3]Narayanan, S., and Shanbhag, R. L., "Acoustoelasticity of a Damped Sandwich Panel Backed by a Cavity," *Journal of Sound and Vibration,* Vol. 78, No. 4, 1981, pp. 453–473.

[4]Bofilios, D. A., and Vaicaitis, R., "Response of Double-Wall Composite Shells to Random Point Loads," *Journal of Aircraft,* Vol. 24, No. 4, 1987, pp. 268–273.

[5]Hong, A. K., and Vaicaitis, R., "Nonlinear Response of Double Wall Sandwich Panels," *Journal of Structural Mechanics,* Vol. 12, 1985, pp. 483–503.

[6]Sathyamoorthy, M., "Nonlinear Vibration Analysis of Plates: A Review and Survey of Current Developments," *Applied Mechanics Reviews,* Vol. 40, No. 11, ASME Book No. AMR027, 1987, pp. 1553–1561.

[7]Yamada, G., and Irie, T., "Plate Vibration Research in Japan," *Applied Mechanics Reviews,* Vol. 40, No. 7, ASME Book No. AMR021, 1987, pp. 879–892.

[8]Timoshenko, S., and Woinowsky-Krieger, S., *Theory of Plates and Shells,* 2nd ed., McGraw-Hill, New York, 1959.

[9]Meirovitch, L., *Analytical Methods in Vibrations,* Macmillan, New York, 1967.

[10]Leissa, A. W., "Plate Vibration Research: Complicating Effects," *Shock and Vibration Digest,* Vol. 13, No. 10, 1981, pp. 19–36.

[11]Lyrintzis, C. S., and Bofilios, D. A., "Moisture Effect on the Response of Orthotropic Stiffened Panel Structures," *AIAA Journal,* Vol. 28, No. 12, 1990, pp. 2117–2124.

[12]Lyrintzis, C. S., and Bofilios, D. A., "Hygrothermal Effects on the Structure-Borne Noise Transmission of Stiffened Laminated Composite Plates," *Journal of Aircraft,* Vol. 27, No. 8, 1990, pp. 722–730.

[13]Vaicaitis, R., "Noise Transmission by Viscoelastic Sandwich Panels," NASA-TND-8516, 1977.

[14]Smolenski, C. P., and Kroksky, E. M., "Dilatational Mode Transmission in Sandwich Panels," *Journal of the Acoustical Society of America,* Vol. 54, No. 6, 1973, pp. 1449–1457.

[15]Bofilios, D. A., and Lyrintzis, C. S., "Structure-Borne Noise Transmission into Cylindrical Enclosures of Finite Extent," *AIAA Journal,* Vol. 29, No. 8, 1991, pp. 1193–1200.

[16]Kunukkasseril, V. X., and Swamidas, A. S. J., "Normal Modes of Elastically Connected Circular Plates," *Journal of Sound and Vibration,* Vol. 30, No. 1, 1973, pp. 99–108.

[17]Chonan, S., "The Free Vibrations of Elastically Connected Circular Plate Systems with Elastically Restrained Edges and Radial Tensions," *Journal of Sound and Vibration,* Vol. 49, No. 1, 1976, pp. 129–136.

[18]Schlack, A. L., Jr., Kessel, W. N., and Dong, W. N., "Dynamic Response of Elastically Supported Circular Plates to a General Surface Load," *AIAA Journal,* Vol. 10, No. 6, 1972, pp. 733–738.

[19]Reismann, H., "Forced Vibrations of a Circular Plate," *Journal of Applied Mechanics,* Vol. 26, *Transactions of American Society of Mechanical Engineers,* Vol. 81, 1959, pp. 526–527.

[20]Wah, T., "Vibration of Circular Plates," *Journal of the Acoustical Society of America,* Vol. 34, No. 3, 1962, pp. 275–281.

[21]Anderson, G., "On the Determination of Finite Integral Transforms for Forced Vibrations of Circular Plates," *Journal of Sound and Vibration,* Vol. 9, No. 1, 1969, pp. 126–144.

[22]Weiner, R. S., "Forced Axisymmetric Motions of Circular Elastic Plates," *Journal of Applied Mechanics,* Vol. 32, *Transactions of American Society of Mechanical Engineers,* Vol. 87, 1965, pp. 893–899.

[23]Leissa, A. W., and Narita, Y., "Natural Frequencies of Simply Supported Circular Plates," *Journal of Sound and Vibration,* Vol. 70, No. 2, 1980, pp. 221–229.

[24]Jacquot, R. G., and Lindsay, J. E., "On the Influence of Poisson's Ratio on Circular Plate Natural Frequencies," *Journal of Sound and Vibration,* Vol. 52, No. 4, 1977, pp. 603–605.

[25]Bert, C. W., and Eagle, M. D., "Dynamics of Composite, Sandwich, and Stiffened Shell-Type Structures," *Journal of Spacecraft and Rockets,* Vol. 6, No. 12, 1969, pp. 1345–1361.

[26]McLachlan, N. W., *Bessel Functions for Engineers,* 2nd ed., Clarendon Press, Oxford, England, UK, 1955.

[27]Lin, Y. K., *Probabilistic Theory of Structural Dynamics,* Robert E. Krieger Publishing, Huntington, NY, 1976, pp. 207–228.

[28]MSC/NASTRAN *Handbook for Dynamic Analysis,* MacNeal-Schwendler, Los Angeles, CA, 1985.

[29]Soedel, W., *Vibrations of Shells and Plates,* Marcell Dekker, 1981.